Structure and Properties of Elastomeric Polypropylene from C_2 and C_{2v}-Symmetric Zirconocenes. The Origin of Crystallinity and Elastic Properties in Poorly Isotactic Polypropylene

Claudio De Rosa,* Finizia Auriemma, and Costantino Perretta

Dipartimento di Chimica, Università di Napoli "Federico II", Complesso Monte S. Angelo, Via Cintia, 80126 Napoli, Italy

Received April 5, 2004; Revised Manuscript Received June 18, 2004

ABSTRACT: A comparative analysis of the structure and mechanical properties of two elastomeric amorphous and semicrystalline polypropylenes samples, produced with C_{2v}-symmetric and chiral C_2-symmetric *ansa*-zirconocene catalysts, respectively, is presented. The poorly isotactic polypropylene (*iam*-PP) of medium molecular weight, prepared with the chiral C_2-symmetric catalyst, slowly crystallizes, by aging at room temperature or by stretching, in a continuum of disordered modifications intermediate between α and γ forms of isotactic polypropylene. Structural and morphological transformations occur during stretching. Disordered α/γ modifications, containing a high fraction of perpendicular chains, present in the unoriented film, transform by stretching at high deformations into structures more similar to the α form with a high content of parallel chains. The development of the small level of crystallinity induces elastic properties. The small crystalline domains in the amorphous matrix, indeed, act as physical knots of the elastomeric lattice. This poorly isotactic *iam*-PP sample shows, instead, poor elastic properties and viscous flow at high deformations in the amorphous state, before crystallization, because of the not high molecular weight. The unique crystallization mode of the *iam*-PP sample explains the remarkable enhancement of elastic properties in low stereoregular polypropylene upon development of crystallinity. The fully amorphous high molecular weight atactic polypropylene (*a*-PP), prepared with the C_{2v}-symmetric catalyst, presents elastic behavior only in a small deformation range (up to 300% strain) and experiences viscous flow of the chains at high deformations. The elasticity arises from the physical network generated by the high degree of entanglement of the polymeric chains generated by the high molecular weight of the sample. The poorly isotactic *iam*-PP sample, before crystallization, presents much poorer elastic properties than the *a*-PP sample because of the lower molecular weight. After crystallization, it shows better elastic properties in a large range of deformation with higher strength, notwithstanding the lower molecular weight, due to the presence of crystallinity.

Introduction

The development of metallocene catalysts for the polymerization of olefins has provided access to new polymer microstructures, and new materials having interesting physical properties, which cannot be obtained with conventional Ziegler−Natta catalysts, have been produced.[1−4] For instance, for polypropylene it is now possible to produce samples with any type and degree of stereoregularity, from highly isotactic to highly syndiotactic polypropylene.[4] In particular, poorly crystalline or amorphous polypropylenes have raised great interest because they show physical and mechanical properties different from those of the stiff plastic highly isotactic polypropylene (i-PP). These low crystalline polypropylenes are, indeed, transparent materials with improved toughness that may present elastomeric properties. Studies of thermoplastic elastomeric polypropylene are of particular interest to extend applications of polypropylene into fields that require improved transparency, toughness, and softness.

The first example of thermoplastic elastomeric polypropylene was described by Natta[5−7] and was obtained by fractionating polypropylenes made with conventional titanium- and vanadium-based Ziegler−Natta catalysts. The elastic properties of this material were interpreted in terms of a stereoblock microstructure of the chains, consisting of alternating blocks of atactic noncrystallizable sequences and more regular isotactic sequences, which are able to crystallize producing a physical crosslinked network.

In recent years, several authors have described new strategies for synthesizing elastomeric polypropylene using different heterogeneous and homogeneous metallocene catalysts. High molecular weight stereoblock polypropylene has been prepared by Collette et al.[8−10] with highly active heterogeneous catalysts consisting of transition-metal alkyls R_4M (where M = Ti, Zr, or Hf and R = benzyl, neopentyl, or neophyl) supported on Al_2O_3. This material is not homogeneous, as fractions of different stereoregularity can be separated by conventional extraction with boiling solvents, but shows elastomeric properties as polymerized. The elasticity is attributed to the high molecular weight fractions containing chains with stereoblock microstructure, with short isotactic crystallizable blocks alternating to longer stereoirregular sequences.[8−10]

Thermoplastic elastomeric polypropylene has recently been obtained with different classes of metallocene catalysts (Chart 1). Unbridged zirconocene catalysts, described by Coates and Waymouth[11,12] (**1** in Chart 1), produce a reactor blend of stereoblock polypropylene which can be separated in fractions of different tacticities and melting temperatures. Elastomeric polypropylene has also been produced by different C_1-symmetric metallocene catalysts described by Chien[13] (**2** in Chart

* To whom correspondence should be addressed. Telephone: ++39 081 674346; fax: ++39 081 674090; e-mail: claudio.derosa@unina.it.

10.1021/ma0493372 CCC: $27.50
Published on Web 08/12/2004

Table 1. Polymerization Temperatures (T_p), Intrinsic Viscosities (IV), Molecular Weights (M_w), Polydispersity Indices (M_w/M_n), Melting Temperatures (T_m), and Content of Pentads Stereosequences (%) of *a*-PP and *iam*-PP Samples Prepared with Catalysts 5 and 6/MAO[19,22]

sample	T_p (°C)	catalyst	IV (dL/g)	M_w[a]	M_w/M_n	[*mmmm*]	[*mmmr*]	[*rmmr*]	[*mmrr*]	[*mmrm*] + [*rmrr*]	[*rmrm*]	[*rrrr*]	[*rrrm*]	[*mrrm*]	T_m (°C)[b]
a-PP	50	**5**	2.57	420 000	2.4	2.6	7.5	6.6	11.8	24.3	12.3	12.2	15.7	6.9	
iam-PP	40	**6**	1.17	143 700	≈2	35.0	17.2	2.5	18.7	7.5	3.2	2.2	3.8	9.9	45

[a] Evaluated from intrinsic viscosities. [b] Peak temperatures from DSC heating scans at 10 °C/min.

Chart 1

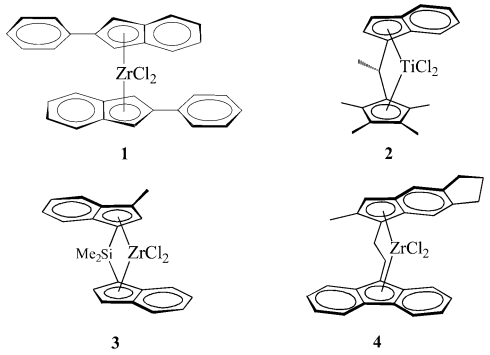

Chart 2

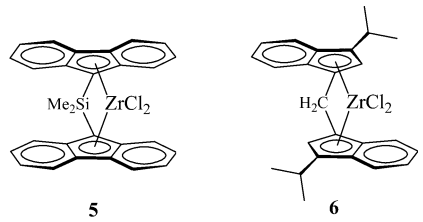

1), Collins[14−17] (**3** in Chart 1), and Rieger[18] (**4** in Chart 1). In these cases, poorly isotactic polypropylene with low melting temperatures or amorphous polypropylenes having a more homogeneous distribution of stereoerrors are obtained.[13−18]

Recently, Resconi has developed C_{2v}-symmetric *ansa*-zirconocene catalysts, such as dimethylsilyl(9-fluorenyl)$_2$ zirconium dichloride ($Me_2Si(9\text{-}Flu)_2ZrCl_2$, complex **5** in Chart 2), that efficiently produces high molecular weight atactic polypropylene (*a*-PP),[19,20] showing elastic behavior.[21]

More recently, Resconi et al.[22,23] has reported a new class of chiral C_2-symmetric *ansa*-zirconocene catalysts of general formula *rac*-$R'_2C(3\text{-}CHR_2\text{-}1\text{-indenyl})_2ZrCl_2$ (for instance, *rac*-$H_2C(3\text{-}i\text{-propyl-}1\text{-indenyl})_2ZrCl_2$, complex **6** in Chart 2), which produce highly flexible, transparent, and nonsticky amorphous polypropylenes with medium molecular weights and a prevailingly isotactic microstructure. Also in these cases the polymers present a random distribution of stereoerrors, which is the major structural difference with the stereoblock polypropylene produced with **1**. The presence of short isotactic sequences allows development of a small level of crystallinity in some of these materials,[22,24] which show some elastic properties.[23] Moreover, these poorly isotactic, almost amorphous, polypropylenes (*iam*-PP) show better miscibility with i-PP compared to atactic polypropylene (*a*-PP), leading to flexible polypropylene blends with improved transparency.[23]

In this paper, an analysis of the structure and mechanical properties of the poorly isotactic polypropylene (*iam*-PP) prepared with catalyst **6** is presented and compared with the physical properties of the fully amorphous atactic polypropylene sample (*a*-PP) prepared with catalyst **5** (Chart 2).

Experimental Section

The atactic polypropylene *a*-PP sample has been prepared in liquid monomer at 50 °C, using the C_{2v}-symmetric catalyst $Me_2Si(9\text{-}Flu)_2ZrCl_2$ (**5** in Chart 2) activated with methylaluminoxane (MAO), as described in ref 19. The poorly isotactic *iam*-PP sample has been prepared in liquid monomer at 40 °C with the chiral C_2-symmetric catalyst *rac*-$H_2C(3\text{-}i\text{-propyl-}1\text{-indenyl})_2ZrCl_2$ (**6** in Chart 2) activated with methylaluminoxane (MAO), as described in ref 22. The intrinsic viscosities, the molecular weights, the melting temperatures, and the microstructural characteristic (distribution of pentads stereosequences) are reported in Table 1.[19,22] It is apparent that the achiral catalyst **5** produces high molecular weight polypropylene, whereas the chiral catalyst **6** produces polypropylene with a slightly lower molecular weight but richer in isotactic *mmmm* pentad content.

Oriented fibers of the *iam*-PP samples have been obtained by stretching at room temperature and at a drawing rate of 10 mm/min crystalline compression molded samples.

X-ray diffraction patterns were obtained with Ni filtered CuKα radiation. The powder profiles were obtained with an automatic Philips diffractometer, whereas the fiber diffraction patterns were recorded on a BAS-MS imaging plate (FUJIFILM) using a cylindrical camera and processed with a digital imaging reader (FUJIBAS 1800). The X-ray fiber diffraction patterns have been recorded for stretched fibers soon after the stretching and keeping the fiber under tension, as well as for relaxed fibers, that is, after keeping the fiber under tension for 2 h and then removing the tension allowing the complete relaxation of the specimens. The index of crystallinity was evaluated from the X-ray powder diffraction profiles by the ratio of the crystalline diffraction area and the total area of the diffraction profile.

The melting temperatures were obtained with a differential scanning calorimeter Perkin-Elmer DSC-7 performing scans in a flowing N_2 atmosphere and heating rate of 10 °C/min.

The intrinsic viscosities were measured in 1,2,3,4-tetrahydronaphthalene solutions at 135 °C, using standard Ubbelohde viscosimeter.

Mechanical tests have been performed at room temperature on compression-molded films and oriented fibers with a miniature mechanical tester apparatus (Minimat, by Rheometrics Scientific), following the standard test method for tensile properties of thin plastic sheeting ASTM D882-83. Compression-molded films have been prepared by heating powder samples at 100 °C between perfectly flat brass plates under a press at very low pressure and slowly cooling to room temperature. Special care has been taken to obtain films with uniform thickness (0.3 mm) and minimal surface roughness, according to the recommendation of the standard ASTM D-2292-85.

Mechanical tests have been first performed on the unstretched compression-molded films. Rectangular specimens 10-mm long, 5-mm wide, and 0.3-mm thick have been stretched up to the break or up to a given strain ϵ. Similar tests have been then performed at room temperature on the strained and stress-relaxed fibers. Stress-relaxed fiber specimens have been prepared by stretching the compression molded films of initial length L_0 up to strains of 300% and 600% for *a*-PP and *iam*-PP samples, respectively (final lengths $L_f = 4L_0$ and $7L_0$, respectively), keeping the fibers under tension for 10 min at room temperature, then removing the tension, allowing the specimens to relax. Mechanical cycles of stretching and relaxation have been performed at room temperature on these stress-relaxed fibers and the corresponding hystereses have

been recorded. In these cycles, the stress-relaxed fibers of *a*-PP and *iam*-PP having the new initial length L_r have been stretched up to the final lengths $L_f = 4L_0$ and $7L_0$, respectively. In the mechanical tests, the ratio between the drawing rate and the initial length was fixed equal to 0.1 mm/(mm×min) for the measurement of Young's modulus and 10 mm/(mm×min) for the measurement of stress−strain curves and the determination of the other mechanical properties (stress and strain at break and tension set). The values of the tension set were measured according to the standard test method ASTM D412-87. The specimens of initial length L_0 were stretched up to a length L_f, that is, up to the elongation $\epsilon = [(L_f - L_0)/L_0]\times 100$, and held at this elongation for 10 min; then the tension was removed, and the final length of the relaxed specimens L_r was measured after 10 min. The tension set was calculated by using the following formula: $t_s(\epsilon) = [(L_r - L_0)/L_0]\times 100$, whereas the elastic recovery was calculated as $r(\epsilon) = [(L_f - L_r)/L_r]\times 100$. The reported values of the mechanical properties are averaged over at least five independent experiments. The stress-relaxation tests were performed on unoriented compression-molded films following the procedure described in the standard test method ASTM D2991-84. Instantaneous strains ϵ were applied and the values of the stress were recorded as a function of the time.

Results and Discussion

The catalyst **5**/MAO shows a high activity in propylene polymerization, producing fully amorphous atactic polypropylene (*a*-PP) of very high molecular weights (Table 1).[19] The catalyst **6**/MAO produces polypropylene (*iam*-PP) with lower molecular weight and a prevailingly isotactic microstructure ([*mmmm*] = 35%, Table 1) with no measurable *regio*-errors (2,1 or 3,1 insertions).[22] Both samples show apparently elastic properties, whereas only *iam*-PP is able to crystallize.[22,24]

Structural Characterization. The ability of the highly stereoirregular *iam*-PP sample to crystallize depends on the microstructure and is in line with the general view of the crystallization properties of metallocene-made i-PP.[24−27]

Isotactic polypropylene crystallizes in three different polymorphic forms (α, *β*, and *γ* forms),[28] characterized by chains in the threefold helical conformation. The polymorphic behavior of metallocene-made i-PP samples, and in particular the relative stability of the α and *γ* forms under common conditions of crystallization, is completely different from that of i-PP samples prepared with heterogeneous Ziegler−Natta catalysts and is closely related to their microstructure.[24−27,29] Commercial i-PP, prepared with the traditional heterogeneous Ziegler−Natta catalytic systems, generally crystallizes in the stable α form.[28] The *γ* forms may be obtained only under special conditions of crystallization, by crystallization from the melt at elevated pressures (about 5000 atm), or by crystallization at atmospheric pressure of low molecular weight samples, and of copolymers containing small amounts (in the range 5−20 mol %) of other olefins.[30]

i-PP samples prepared with homogeneous metallocene catalysts crystallize instead more easily in the *γ* form, even at atmospheric pressure and for high molecular weight samples.[25−27,29] The different crystallization behavior is due to the different microstructures of the chains of metallocene-made and Ziegler−Natta i-PP and, in particular, to the different distribution of defects of stereoregularity or regioregularity produced by the different types of catalytic system.

In recent papers, it has been clearly shown that when the fully isotactic sequences are very short, i-PP crystallizes in the *γ* form, whereas very long regular isotactic sequences generally crystallize only in the α form.[25−27] In chains of i-PP samples prepared with single center metallocene catalysts, the distribution of defects is random and the length of fully isotactic sequences is roughly inversely related to the content of insertion errors.[25−27] As a consequence, even a small amount of defects reduces the length of the regular isotactic sequences inducing the crystallization of the *γ* form.[25−27] The content of *γ* form increases with increasing concentration of defects because of the reduced length of the regular isotactic sequences.[26]

For this reason, metallocene-made i-PP generally crystallizes in mixture of α and *γ* forms; the relative content of the two polymorphs depends on the crystallization temperature and the stereoregularity of the sample. However, in most of the crystallization conditions modifications containing high degrees of structural disorder are obtained.[24,26] A model of such a disordered modification is reported in Figure 1 in comparison with the limit-ordered models of the α (Figure 1A) and *γ* (Figure 1C) forms. The limit-ordered structure model proposed for the *γ* form is characterized by a regular packing along the c_γ direction of bilayers of chains with axes oriented alternatively along two nearly perpendicular directions (Figure 1C).[31] Crystals of the *γ* form obtained in the metallocene-made i-PP samples instead present structural disorder,[24,26] characterized by defects in the regular stacking of bilayers of chains (Figure 1B). Consecutive bilayers may face each other with the chain axes either parallel (like in the α form, Figure 1A) or nearly perpendicular (like in the *γ* form, Figure 1C). In this model of disordered structure (Figure 1B), ordered domains in α or *γ* forms are present inside the same crystal, giving rise to a mixture at molecular level of the α and *γ* forms. The disordered structure (Figure 1B) can be considered as an intermediate modification between the two ordered α and *γ* forms. In refs 24 and 26, we have shown that different disordered modifications, containing different amounts of α-like or *γ*-like arrangements of the chains, can be obtained depending on the crystallization conditions and stereoregularity of the sample. Therefore, metallocene i-PP crystallizes in a continuum of disordered modifications intermediate between α and *γ* forms, the amount of disorder being dependent on the crystallization conditions and on the stereoregularity of the sample.[26]

The X-ray powder diffraction profiles of *a*-PP and *iam*-PP samples are shown in Figure 2. It is apparent that while *a*-PP is totally amorphous the poorly isotactic *iam*-PP sample presents a small crystallinity. The as-prepared *iam*-PP sample is actually amorphous and does not crystallize by cooling the melt to room temperature. It slowly crystallizes if the sample cooled from the melt is kept at room temperature for several days. The X-ray powder diffraction profiles of the sample *iam*-PP cooled from the melt to room temperature and kept at room temperature for different times up to the complete crystallization are reported in Figure 3. The maximum level of crystallinity, achieved after one week aging at room temperature, is very small and corresponds to a crystallinity index of nearly 16% with a melting temperature of 45 °C.

The X-ray diffraction profile of the *iam*-PP sample of Figures 2b and 3d is characterized by the presence of a sharp diffraction peak at $2\theta = 17°$ and two broad maxima at $2\theta \approx 14°$ and $2\theta = 18°-21°$. The sharp peak

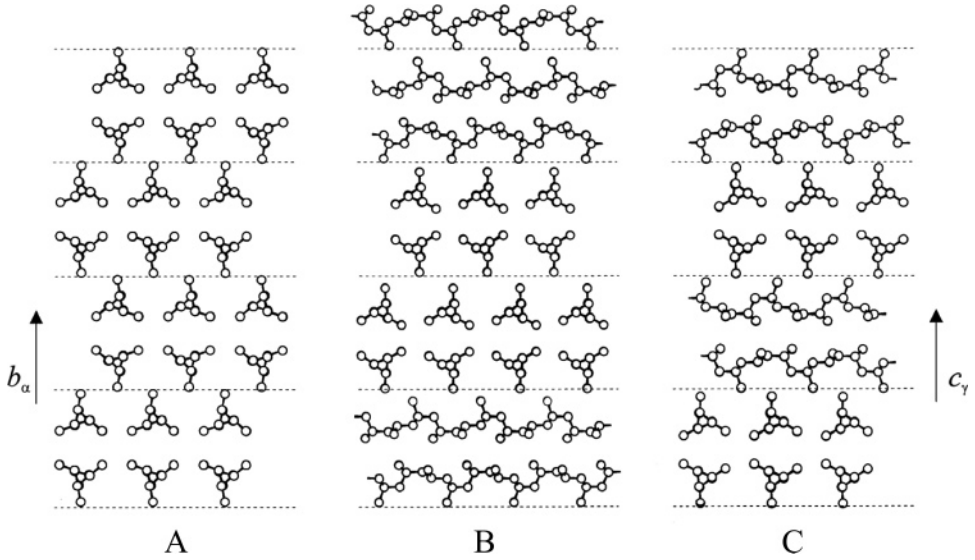

Figure 1. Limit-ordered models of packing proposed for α (A) and γ (C) forms of i-PP and model of the α/γ disordered modifications intermediate between the α and γ forms (B). The dashed horizontal lines delimit bilayers of chains. Subscripts α and γ identify unit cell parameters referred to the monoclinic and orthorhombic unit cells of α and γ forms, respectively. In the disordered model (B), consecutive bilayers of chains are stacked along b_α (c_γ) with the chain axes either parallel or nearly perpendicular, making α-like or γ-like arrangements of bilayers.

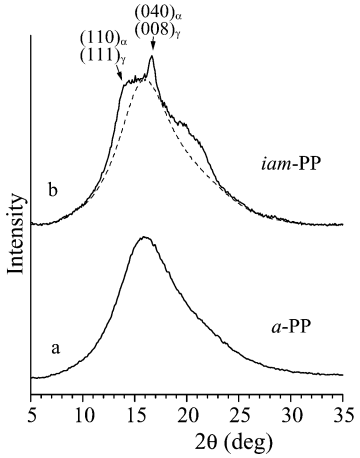

Figure 2. X-ray powder diffraction profiles of the *a*-PP (profile a) and *iam*-PP (profile b) samples. The $(110)_\alpha$ and $(111)_\gamma$ reflections at $2\theta = 14°$ of α and γ forms, respectively, and the $(040)_\alpha$ and $(008)_\gamma$ reflections at $2\theta = 17°$ of α and γ forms of i-PP, respectively, are indicated. In b the dashed line indicates the diffraction profile of the amorphous phase.

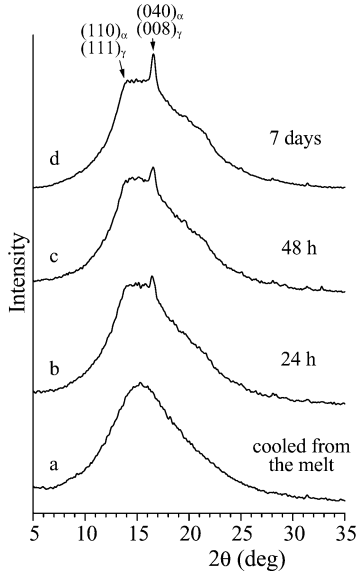

Figure 3. X-ray powder diffraction profiles of the sample *iam*-PP cooled from the melt and kept at room temperature for the indicated time. The $(110)_\alpha$ and $(111)_\gamma$ reflections at $2\theta = 14°$ of α and γ forms, respectively, and the $(040)_\alpha$ and $(008)_\gamma$ reflections at $2\theta = 17°$ of α and γ forms of i-PP, respectively, are indicated.

at $2\theta = 17°$ is common to α and γ forms of i-PP and corresponds to the $(040)_\alpha$ reflection of the α form or the $(008)_\gamma$ reflection of the γ form. The broad maximum at $2\theta \approx 14°$ is in the region corresponding to the $(110)_\alpha$ and $(111)_\gamma$ reflections of α and γ forms, respectively, whereas the second broad maximum at $2\theta = 18°-21°$ includes the $(130)_\alpha$ reflection at $2\theta = 18.6°$ of the α form and the $(117)_\gamma$ reflection at $2\theta = 20.1°$ of the γ form. The presence of only the sharp $(040)_\alpha$ or $(008)_\gamma$ reflection at $2\theta = 17°$, and the absence of other sharp Bragg reflections of both α and γ forms, as $(110)_\alpha$ and $(130)_\alpha$ reflections at $2\theta = 14°$ and 18.6°, respectively, typical of the α form,[28] and $(111)_\gamma$ and $(117)_\gamma$ at $2\theta = 14$ and 20.1°, respectively, typical of the γ form,[31] indicates that the *iam*-PP sample does not crystallize in the pure α or γ forms. These data indicate that the sample is crystallized in an α/γ disordered modification of the kind shown in Figure 1B, containing disorder in the stacking along the b_α or c_γ direction of bilayers of chains with axes either parallel or perpendicular.[24,26] In fact, as demonstrated in refs 24 and 26, the presence of this disorder produces a strong decrease of the intensities of $(110)_\alpha$ and $(130)_\alpha$ reflections of the α form at $2\theta = 14°$ and 18.6°, respectively, and of the $(117)_\gamma$ reflection of the γ form at $2\theta = 20.1°$, as actually occurs for the sample *iam*-PP (Figure 2b). The whole X-ray diffraction pattern of the sample *iam*-PP can be well-reproduced with a disordered structure model containing a slight prevalence (nearly 60%) of consecutive bilayers having perpendicular chains.[24]

Oriented fibers of the *iam*-PP sample have been obtained by stretching at room temperature and at a drawing rate of 10 mm/min compression molded samples after achieving the complete crystallization. Compression molded films have been kept at room temperature for at least one week before stretching. The X-ray fiber

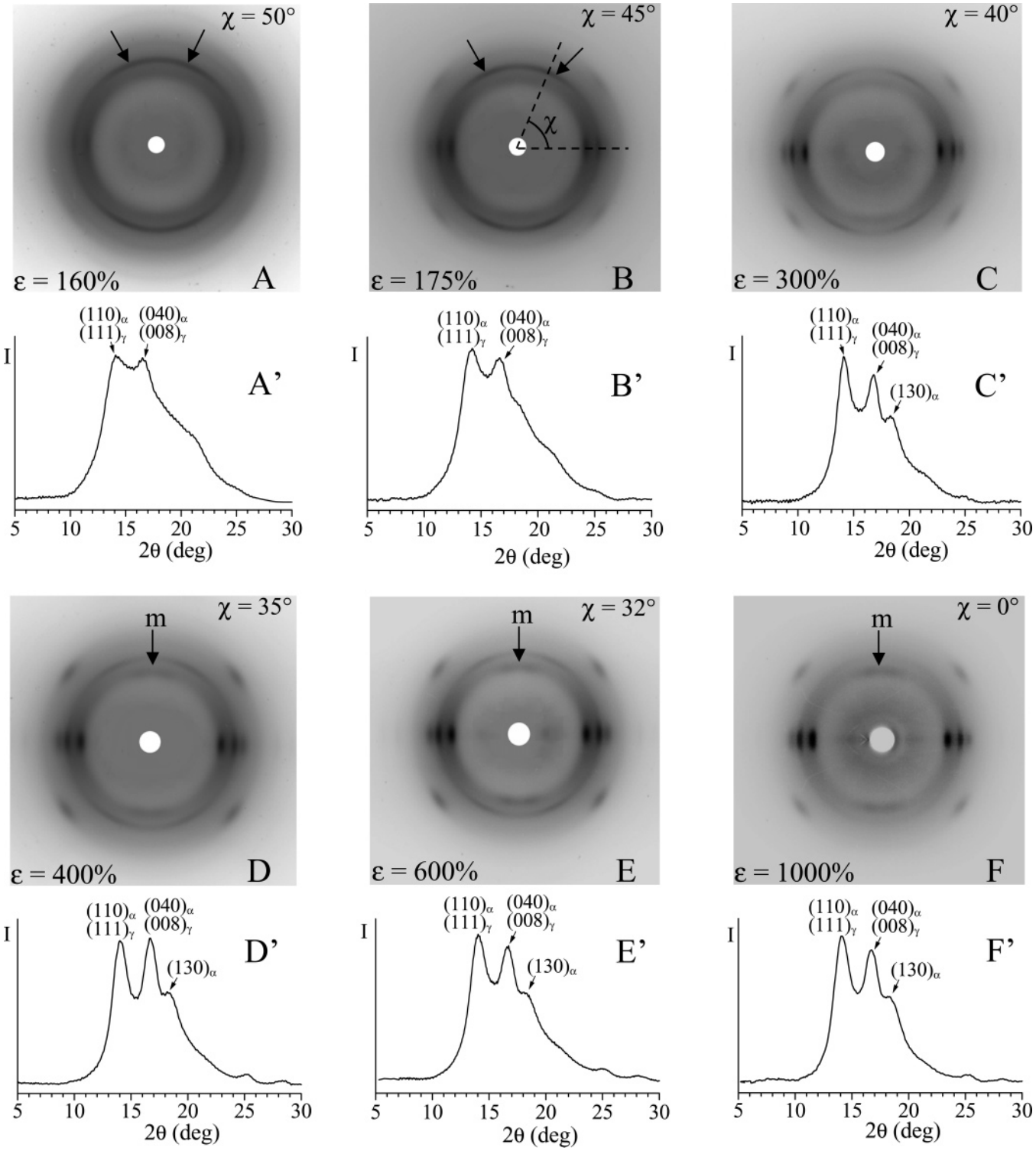

Figure 4. X-ray fiber diffraction patterns (A−F), and corresponding profiles read along the equatorial lines (A′−F′), of fibers of the sample *iam*-PP obtained by stretching at room temperature compression molded films at values of the strain ϵ of 160% (A), 175% (B), 300% (C), 400% (D), 600% (E), and 1000% (F). The $(110)_\alpha$, $(040)_\alpha$, and $(130)_\alpha$ reflections of the α form at $2\theta = 14$, 17, and 18.6°, respectively, and $(111)_\gamma$ and $(008)_\gamma$ reflections of the γ form at $2\theta = 14$ and 17°, respectively, are indicated. The meridional $(111)_\gamma$ or $(110)_\alpha$ reflection at $2\theta = 14°$ is indicated with "m" in D−F. The values of the azimuthal angle χ, defined in B, of the reflection at $2\theta = 17°$ indicated by arrows in A and B are also shown.

diffraction patterns of fiber specimens of the sample *iam*-PP obtained by stretching at different draw ratios, keeping the fibers under tension, are reported in Figure 4. The corresponding intensity profiles read along the equatorial line are also reported in Figure 4. As described in ref 24, oriented fibers of the sample *iam*-PP are also characterized by α/γ disordered modifications (Figure 1B) intermediate between α and γ forms. The X-ray fiber diffraction patterns of fibers obtained at low deformations ($\epsilon \leq 170\%$) present reflections at $2\theta = 14°$, 17°, and 20° slightly polarized on the equator with a low degree of orientation of crystals (Figure 4A). The presence in the diffraction pattern of Figure 4A of the broad reflection at $2\theta = 20°$, corresponding to the $(117)_\gamma$ reflection of the γ form, although very broad and of low intensity, and the absence of the $(130)_\alpha$ reflection of the

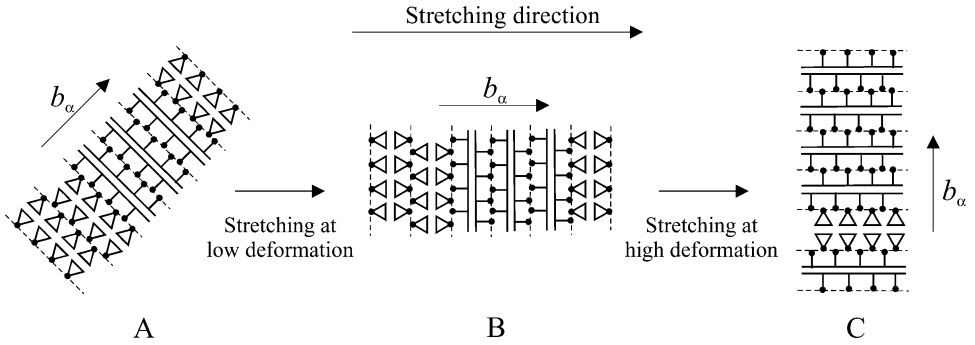

Figure 5. Schematic representation of the structural and morphological transformation occurring by stretching the *iam*-PP sample. The triangles indicate chains of i-PP in threefold helical conformation in a projection with the chain axes perpendicular to the plane of the drawing. The continuous lines indicate chains of i-PP with the chain axes in the plane of the drawing, whereas the filled balls indicate the methyl groups. The dashed lines delimit adjacent bilayers of chains. (A) Randomly oriented crystalline domain present in the unstretched film. The crystals are characterized by α/γ disordered modifications containing a nearly statistical succession along the b_α axis of bilayers having parallel chains (as in the α form) or perpendicular chains (as in the γ form). (B) By stretching at low values of deformation, crystals in α/γ disordered modifications are oriented with the two chain axes perpendicular to the stretching direction and the b_α axis oriented parallel to the stretching direction. (C) By stretching at high values of deformation, the α/γ disordered modifications transform into modifications more similar to the α form with an increase of the fraction of parallel chains and, contemporarily, crystals are oriented with the chain axes parallel to the stretching direction as in a standard fiber orientation.

α form at $2\theta = 18.6°$, indicate that, as in the unoriented film (Figure 3), the crystalline phase of fibers stretched at low deformations is characterized by α/γ disordered modifications (Figure 1B) with a higher fraction (nearly 60−70%) of consecutive bilayers having perpendicular chains, as in the γ form.

With increasing deformation ($\epsilon > 170\%$), the degree of orientation of crystals increases, as indicated by the increase of the polarization of the reflections on the equator in the diffraction patterns of Figure 4B−F. Moreover, a decrease of the intensity of the reflection at $2\theta = 20°$ and an increase of the intensity at $2\theta = 18.6°$, corresponding to the reflection $(130)_\alpha$ of the α form, is observed with increasing deformation (Figure 4C−F). This indicates that fibers stretched at higher deformations are still in α/γ disordered modifications but with a higher fraction of consecutive bilayers having parallel chains, as in the α form.

The fiber diffraction patterns of Figure 4 indicate that the sample *iam*-PP undergoes a structural transformation during stretching. Disordered modifications of the kind of Figure 1B closer to the γ form, characterized by a prevalence of local packing typical of the γ form with perpendicular chains, obtained at low deformations ($\epsilon \leq 170\%$), transform by stretching at high deformations into disordered modifications closer to the α form, characterized by a prevalence of local packing typical of the α form with parallel chains.

Diffraction patterns similar to those of Figure 4A and B have been obtained by stretching at low degrees of deformation ($\epsilon < 170\%$) amorphous compression molded films of the *iam*-PP sample before occurrence of crystallization at room temperature. In this condition, the samples crystallize by stretching or by aging under stretching in similar α/γ disordered modifications. However, in this condition the samples show low toughness because of the noncomplete crystallization and break at deformations higher than 200%.

In the X-ray diffraction patterns of *iam*-PP fibers stretched at low deformations ($\epsilon < 300\%$), the second equatorial reflection at $2\theta = 17°$ appears more polarized on the region close to the meridian (reflections indicates by arrows in Figure 4A−B). The position of this reflection may be indicated by the azimuthal coordinate χ defined in Figure 4B ($\chi = 0$ and 90° for equatorial and meridional reflections, respectively). The value of the azimuthal coordinate is 50° for the fiber stretched at 160% deformation (Figure 4A) and decreases with increasing deformation (Figure 4B−F). At deformations higher than 160%, this reflection appears polarized either on the equator ($\chi = 0$) or on off-equatorial layer lines ($\chi \neq 0$, Figure 4B−E). The intensity on off-equatorial lines decreases whereas that on the equator increases with increasing deformation (Figure 4B−F). At very high deformation ($\epsilon = 1000\%$), the reflection at $2\theta = 17°$ is polarized only on the equator ($\chi = 0$).

We recall that the reflection at $2\theta = 17°$ corresponds to the $(040)_\alpha$ reflection for the α form and the $(008)_\gamma$ reflection for the γ form. This reflection corresponds to crystallographic planes perpendicular to the b_α axis in the α form (Figure 1A) or perpendicular to the c_γ axis in the γ form (Figure 1C). For both polymorphic forms, these crystallographic planes are parallel to the bilayers of chains (dashed lines in Figure 1) and perpendicular to the direction of stacking of bilayers. The polarization of this reflection on off-equatorial lines ($\chi \neq 0$) at low deformations (Figure 4A−B) indicates that a nonstandard fiber orientation of crystals has been obtained, that is, the presence of crystals having the axes of stacking of bilayers of chains (b_α or c_γ axes, Figure 1) oriented preferably along the stretching direction. In this orientation, the polymeric chains are oriented in directions perpendicular to the stretching direction. The amount of crystals oriented with chain axes perpendicular to the stretching direction decreases with increasing deformation, as indicated by the decrease of the intensity of the reflection at $\chi \neq 0$, on off-equatorial lines, with increasing deformation ($\epsilon > 300\%$, Figure 4C−F). Contemporarily, the reflection moves to lower values of χ with increasing deformation up to $\chi = 0$ at $\epsilon = 1000\%$ (the reflection is present only on the equator, Figure 4F). This indicates that at very high deformation a standard fiber orientation of the crystals is obtained with the chain axes oriented along the stretching direction.

The data of Figure 4 indicate that structural and morphological transformations occur during stretching. A scheme of this transformation is shown in Figure 5. As discussed above, the isotropic unoriented film is in a disordered modification of the γ form with a nearly statistical succession of bilayers of chains having paral-

lel and perpendicular chains. In each of the randomly oriented crystalline domains (for instance, the one shown in Figure 5A), a nearly similar fraction of parallel and perpendicular polymeric chains are present. These crystallites have small dimensions and appear mainly elongated along the b_α (or c_γ) direction, as evidenced by the sharp peak at $2\theta \approx 17°$ in the X-ray diffraction pattern of Figure 2b. Upon stretching the material at small values of deformation ($\epsilon < 300\%$), the crystalline phase is still characterized by disordered modifications close to the γ form. Since these crystallites are elongated entities with chain axes running along two perpendicular directions, both at right angle to the long axis (b_α or c_γ), the crystals tend to orient with this long axis (direction of stacking of bilayers of chains, Figure 1B) aligned parallel to the stretching direction (Figure 5B) and, therefore, with the chain axes perpendicular to the stretching direction. This unusual orientation of polymer crystals is further stabilized by the fact that at small deformations the crystallites are still in disordered modifications of the γ form, with a prevalence of γ-like arrangements of chains with perpendicular axes. Since in each crystalline domain the chains are oriented along two perpendicular directions, the crystals remain anchored with chain axes orthogonal to the stretching direction up to high values of deformations (Figure 4B−E).

By stretching at higher deformations, the disordered modifications close to the γ form transforms into modifications more similar to the α form with an increase of the amount of parallel chains. Since the chains are almost all parallel, the deformation also induces orientation of crystals with the macromolecular chain axes oriented along the stretching direction, as in a standard fiber morphology (Figure 5C).

A similar behavior has been well known for many years in some naturally occurring fibrous proteins such as silks. The perpendicular orientation of chain axes with respect to the fiber axis, described as cross-β,[32] has been explained by the fact that in these soft silks the small crystallites are elongated along the hydrogen bond directions, which run perpendicular to chain axes.[32] In these proteins, the chain axes in the crystallites are linked together by short "bent" regions to form continuous folded polypeptide chains; the bent portions of chains lie in planes normal to the surface of the crystallites and parallel to their long axis (along the H-bond directions). Since these crystallites are elongated entities, they align first with the H-bond directions parallel to the fiber axis, such that the chain axes run perpendicular to the fiber axis.[32] On further stretching, the crystallites are destroyed and the chains become oriented parallel to the stretching direction.[32] This behavior seems very reminiscent of that observed for the small elongated crystals of the α/γ modifications of the *iam*-PP sample (Figures 4 and 5).

The diffraction patterns of Figure 4 present a reflection at $2\theta = 14°$ on the first layer line in a nearly meridional position (reflection indicated with "m" in Figure 4D−F). This reflection could correspond to the $(111)_\gamma$ reflection of the γ form at $2\theta = 14°$. In fact, in the orientation of the crystals with one of the two directions of the chains oriented along the stretching direction, the $(111)_\gamma$ reflection is split into two reflections, one polarized on the equator, the second on the meridian,[24] as found in the experimental patterns of Figure 4. However, the reflection at $2\theta = 14°$ on the meridian could also correspond to the $(110)_\alpha$ reflection of the α form arising from the presence of tilted lamellae of the α form, that is, daughter lamellae of α form grown on mother lamellae of α form with the *c* axis of daughter lamellae oriented along the *a* axis of the mother ones.[30] This crosshatched morphology is typical of crystals of the α form crystallized from the melt or in oriented fibers.[30] Therefore, the presence of nonnegligible amount of tilted lamellae of the α form also in fibers of Figure 4 cannot be excluded.

The X-ray diffraction patterns of fibers of the *iam*-PP sample stretched at 1000% deformation and after releasing the tension are reported in Figure 6. As discussed above, fibers stretched at high values of deformation are in α/γ disordered modifications close to the α form, that is, with a prevalence of α-like arrangement of bilayers of chains (Figures 4F, 6A). Upon releasing the tension, besides a slight decrease of the degree of orientation, a decrease of the intensity of the reflections at $2\theta = 14°$ and 18° of the α form, corresponding to $(110)_\alpha$ and $(130)_\alpha$ reflections, respectively, is observed (Figure 6B). In particular, the diffraction peak at $2\theta = 18°$ present in the pattern of Figure 6A transforms into a broad halo after removing the tension (Figure 6B). This indicates that the relaxation of the fiber sample induces structural or morphological rearrangements involving increase of structural disorder or, probably, a decrease of crystal size that produces broadening of the $(110)_\alpha$ and $(130)_\alpha$ reflections (Figure 6B). The transformation of the α/γ disordered modification close to the α form (Figure 6A), obtained by stretching, into an α/γ disordered modification containing higher fraction of γ-like arrangements upon releasing the tension may be also possible through a relaxation mechanism which involves rearrangement of crystals and even partial melting and recrystallization with formation of a structure very similar to that of the unstretched film (Figure 2b).

Both diffraction patterns of Figure 6 presents the reflection at $2\theta = 14°$ polarized on both equatorial and meridional lines. This indicates that for the relaxed fiber crystals of α/γ disordered modifications are mainly oriented with one of the two directions of the chains oriented along the stretching direction. However, also in this case the presence of nonnegligible amount of tilted lamellae of the α form cannot be excluded.

These data indicate that the poorly isotactic *iam*-PP sample crystallizes in the bulk and in stretched fibers in a continuum of disordered modifications of the kind of Figure 1B intermediate between α and γ forms. The amount of α-like (with parallel chains) and γ-like arrangements (with perpendicular chains) present in these structures changes with the degree of deformation.

This crystallization mode of i-PP explains the observed capability of the *iam*-PP sample to crystallize, even though the stereoregularity of the sample is very low. The ^{13}C NMR analysis has indeed shown that the polymer chains contain a high concentration of defects of stereoregularity, mainly constituted by *rr* triads, and the content of the isotactic pentad *mmmm* is only 35% with an average length of the isotactic sequence of only five monomeric units.[22] The observed crystallization of this sample resides on this particular microstructure and the unique crystallization mode of metallocene-made i-PP (Figure 1).

It has been recently suggested that defects of stereoregularity, such as isolated *rr* triads, can be easily

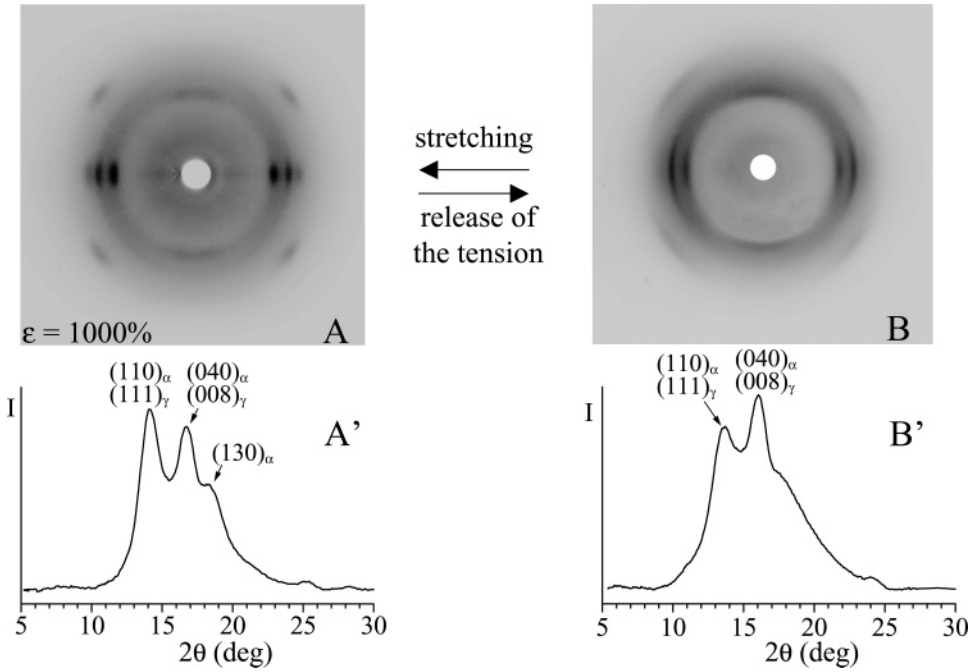

Figure 6. X-ray fiber diffraction patterns (A−B), and corresponding profiles read along the equatorial lines (A′−B′), of fibers of the sample *iam*-PP obtained by stretching at room temperature compression molded films at $\epsilon = 1000\%$ (A) and after releasing the tension (B). The $(110)_\alpha$, $(040)_\alpha$, and $(130)_\alpha$ reflections of the α form at $2\theta = 14$, 17, and 18.6°, respectively, and $(111)_\gamma$ and $(008)_\gamma$ reflections of the γ form at $2\theta = 14$ and 17°, respectively, are indicated.

tolerated at low cost of conformational and packing energy in the crystal lattices of the polymorphic forms of i-PP and of the α/γ disordered modifications of Figure 1B.[24,26,33] In a low conformational energy model of i-PP chains containing *rr* defects, proposed in ref 24, the presence of these defects produces inversion of the chirality of the threefold helix and a bending of the chain.[24] The energy cost for this helix reversal due to the *rr* dyad defect is only about 2 kcal/mol, as evaluated in the literature.[34] Because of the bending of the chain, helix reversals are generally agreed in the past literature not to occur in the crystal lattice of the α form of i-PP, notwithstanding the low energy cost.[34] In the hypothesis suggested in ref 24, this bent defective chain, with helix reversals, could be instead accommodated in the lattices of the γ form and α/γ disordered modifications of i-PP. This is only a hypothesis, not yet supported by packing energy calculations, based on the easy matching of methyl groups of the bent chains with those of neighboring chains,[24] as occurs in the crystal structure of the γ form (Figure 1C).[31]

The *rr* punctual defects may be also included in crystals of α form of i-PP, as indicated by results of solid-state ^{13}CNMR experiments.[33] In a low energy model of conformation of i-PP chain containing an *rr* defect, suitable for packing in crystals of α form,[35] the chain stems connected by the punctual *rr* defect have the same chirality and maintain the same axis. The resulting chain is straight and the destabilization of the helix due to the *rr* triad sequence is about 4 kcal/mol.[34] This kind of conformations could be, however, easily accommodated also in crystals of the γ form. Also in this case this is only a reasonable hypothesis not yet supported by calculations of packing energy. The bent conformations having helical stems connected by the *rr* defect with opposite chirality have, however, lower energy[34] and could be probably easily accommodated only in crystals of the γ form or in α/γ disordered modifications of Figure 1B, not in the α form. This suggests that *rr* defects are possibly present in both α and γ form crystals, but the inclusion in the γ form or in α/γ disordered modifications of Figure 1B is more probable.

This model of inclusion of *rr* defects in the crystals of i-PP introduces a possible mechanism inducing in the poorly isotactic polypropylene samples the observed tendency to crystallize in disordered modifications intermediate between α and γ forms of i-PP. Moreover, this gives a possible explanation of the observed crystallinity in i-PP samples having very low stereoregularity and, as a consequence, of the development of elastic properties, as shown in the next section.

Mechanical Properties. The stress−strain curves of unoriented compression molded films of the semicrystalline *iam*-PP sample and the amorphous *a*-PP sample of Figure 2, stretched at room temperature, are reported in Figure 7. In the *iam*-PP sample, the mechanical tests have been performed on compression molded films after achieving the complete crystallization. Compression molded films have been kept at room temperature for at least one week before the test.

It is apparent from Figure 7 that the amorphous *a*-PP sample presents a nearly linear stress−strain curve at low values of deformation (up to $\epsilon = 100-200\%$). In this deformation range, the sample shows elastic behavior. A maximum value of stress is observed at $\epsilon = 300\%$ (Figure 7A). With increasing deformation for values higher than 300%, a decrease of the stress is observed without breaking, indicating the occurrence of viscous flow of the chains (Figure 7A). Breaking is, indeed, observed only at deformation higher than 7000%.

The semicrystalline *iam*-PP sample presents a stress−strain curve typical of elastomeric materials (Figure 7B), with a small yielding at $\epsilon \approx 100\%$ and high deformation at break. Strain-hardening at high deformations, typical of elastomers, is observed.

The mechanical properties (Young's modulus, stress and strain at break, stress and strain at yield, and

Table 2. Molecular Weight (M_w), Young's Modulus (E), Stress (σ_y) and Strain (ϵ_y) at the Yield Point, Stress (σ_b) and Strain (ϵ_b) at Break, and Crystallinity (x_c) of Compression Molded Films of *a*-PP and *iam*-PP Samples

Sample	M_w	E (MPa)	σ_y (MPa)	ϵ_y (%)	σ_b(MPa)	ϵ_b (%)	x_c(%)[a]
a-PP	420 000	1.1 ± 0.2	0.9 ± 0.2	300 ± 10		>7000	
iam-PP	143 700	1.3 ± 0.6	1.0 ± 0.2	120 ± 10	6 ± 1	1180 ± 57	16

[a] From the X-ray powder diffraction profile.

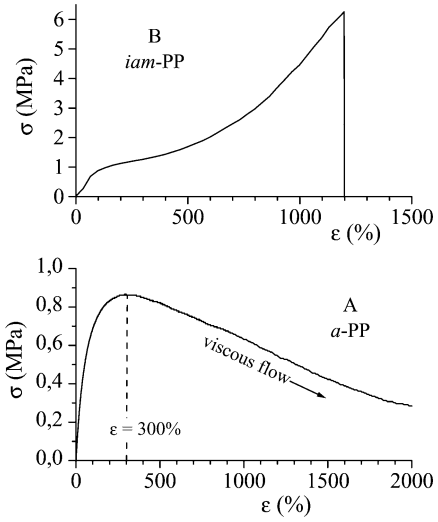

Figure 7. Stress−strain curves of compression molded films of the amorphous *a*-PP sample (A) and of the semicrystalline *iam*-PP sample (B).

tension set at break) of *a*-PP and *iam*-PP samples are reported in Table 2.

Similar values of the elastic modulus have been obtained for the amorphous *a*-PP and poorly crystalline *iam*-PP samples. However, because of the presence of crystallinity, the values of the stress at any strain for the *iam*-PP sample are 1 order of magnitude higher than those of the amorphous *a*-PP sample (Figure 7), and a remarkable value of the tensile strength $\sigma_b = 6$ MPa is observed (Figure 7B, Table 2).

The stress−strain curve of the amorphous *iam*-PP sample, before occurrence of crystallization at room temperature, is similar to that of the amorphous *a*-PP sample at low values of deformation, with low values of the stress at any strain. Because of the lower molecular weight, viscous flow and breaking occur when high deformations (ϵ > 200%) are achieved before complete crystallization.

The values of the tension set, $t_s(\epsilon) = [(L_r - L_0)/L_0] \times 100$ measured at room temperature for unoriented films stretched up to different values of the deformation ϵ, or up to the break (t_b), are reported in Table 3. These values have been obtained by stretching the unoriented films of initial length L_0 up to the break, as in Figure 7, or up to final lengths $L_f = (\epsilon + 1)L_0$, keeping the specimens in tension for 10 min, then removing the tension and measuring the final length L_r of the relaxed sample after 10 min.

The amorphous *a*-PP sample shows low values of tension set only after small deformations, lower than 300%. This indicates that in this small range of deformation the sample shows good elastic properties. For values of deformation higher than 300% the tension set increases, indicating a decrease of the elastic recovery. These data indicate that the elastic properties of the amorphous *a*-PP sample are lost when the sample is stretched at high deformation. This behavior can be explained assuming that the elasticity in the amorphous *a*-PP sample arises from the physical network generated by the high degree of entanglement of the polymeric chains because of the high molecular weight of the sample. The presence of these physical knots, associated with the high viscosity due to the high molecular weight, prevents the viscous flow of the chains when the sample is stretched up to 300% deformation, and a good elastic recovery is observed upon releasing the tension. When the sample is stretched at deformations higher than 300% disentanglement of the chains occurs producing viscous flow (Figure 7) and the sample loses the elastic properties.

In the semicrystalline *iam*-PP sample, low values of the tension set are observed even at high deformation (Table 3), indicating that the *iam*-PP sample experiences a recovery of the initial dimension either after breaking or after removing the tension from any deformation. A slight increase of the tension set is observed with increasing deformation, and values of tension set higher than that observed after breaking are obtained for values of deformation higher than 400%. This is probably because the tension set after a given deformation ϵ has been measured after keeping the sample in tension for 10 min, allowing the sample to relax.

These data indicate that the *iam*-PP sample presents good elastic properties in a large range of deformation. Although the *iam*-PP sample has a molecular weight lower than that of the amorphous *a*-PP sample, it shows better elastic properties. The elasticity of the poorly crystalline *iam*-PP sample is due to the presence of small crystalline domains in the amorphous matrix. The sample is, indeed, mainly amorphous with a small level of crystallinity which develops by aging at room temperature (Figure 3) or by stretching (Figure 4). The small crystalline domains act as physical knots of the elastomeric lattice, preventing the viscous flow of the amorphous chains and giving a typical thermoplastic elastomeric behavior.

In the amorphous *a*-PP samples, the high molecular weight is responsible for the elastic recovery, since it guarantees a high degree of entanglement of the chains, but is not sufficient to prevent the viscous flow at high deformations. In the *iam*-PP sample, the molecular weight is not very high but the very small level of crystallinity produces the formation of a more stable elastomeric network and, moreover, induces higher strength (Figure 7B and Table 2). As discussed in the previous section, the capability of the *iam*-PP sample to crystallize, because of the inclusion of most of the *stereo*-defects in the crystals and the unique crystallization mode of i-PP in a continuum of α/γ disordered modifications (Figure 1), induces elastic properties in i-PP and produces interesting thermoplastic elastomers with high strength.

Moreover, as demonstrated by the structural analysis reported in the previous section, during stretching, besides the morphological transformation which produces oriented fibers, a structural transition from disordered modifications similar to the γ form into disordered modifications more similar to the α form

Table 3. Values of the Tension Set after Breaking (t_b) and Tension Set ($t_s(\epsilon)$) after Deformation ϵ for Unoriented Compression Molded Films of *a*-PP and *iam*-PP Samples[a]

Sample	t_s(100) (%)	t_s(200) (%)	t_s(300) (%)	t_s(400) (%)	t_s(600) (%)	t_s(1000) (%)	t_b (%)
a-PP	14 ± 3	27 ± 2	36 ± 4			370 ± 69	
iam-PP	6 ± 1			31 ± 2	51 ± 3	130 ± 5	30 ± 5

[a] Samples of initial length L_0 are stretched up to the break or up to strains ϵ (final lengths $L_f = (\epsilon+1)L_0$), kept in tension for 10 min at room temperature and then relaxed by releasing the tension.

occurs inside the crystalline domains (Figures 4 and 5). The increase of the fraction of α-like arrangement with chains parallel and oriented along the stretching direction induces, at least in part, the strong strain-hardening of the sample observed at high deformation (Figure 7B), giving rise to the remarkable value of the tensile strength.

It is worth emphasizing, however, that, since the melting temperature of the *iam*-PP sample is rather low (45 °C), the described outstanding mechanical properties are valid at room temperature. At higher temperatures a behavior similar to that of the amorphous *a*-PP sample is expected.

To quantify the elastic properties of *a*-PP and *iam*-PP samples, mechanical cycles of stretching and relaxation have been performed at room temperature on oriented stress-relaxed fibers and the corresponding hysteresis has been recorded. Stress-relaxed fiber specimens have been prepared by stretching the compression molded films up to 300% (for *a*-PP sample) and 600% (for *iam*-PP sample) deformations, keeping the fibers under tension for 10 min at room temperature, then removing the tension, allowing the specimens to relax. The hysteresis cycles, composed of the stress−strain curves recorded during the stretching, immediately followed by the curves recorded during the relaxation at controlled rate, for the fibers of *a*-PP and *iam*-PP samples are reported in Figure 8.

In these cycles, stress-relaxed oriented fibers having the new initial length L_r of the samples *a*-PP and *iam*-PP are stretched up to the final lengths $L_f = 4L_0$ for the sample *a*-PP and $L_f = 7L_0$ for the sample *iam*-PP, with L_0 the initial length of the unoriented film. For each fiber, four successive cycles have been recorded, and each cycle is performed 10 min after the end of the previous cycle. Successive hysteresis cycles, measured after the first one, are all nearly coincident, indicating a tension set close to zero and a perfect elastic recovery. In the fibers of amorphous *a*-PP sample, the residual tension set between the first and second hysteresis cycles is around 2−3% and becomes close to zero starting from the second cycle, the successive cycles, measured after the first one, being all nearly coincident, whereas the average dissipated energy is nearly 20%. In the crystalline *iam*-PP sample, the value of the tension set is 15% after the first cycle and becomes zero starting from the second cycle, whereas the hystereses are nearly zero in all cycles (Figure 8).

Because of the increased disentanglement occurring in the *a*-PP sample with increasing deformation for values higher than 300% strain, the amorphous *a*-PP shows elastic properties in a small range of deformation. Fibers of the crystalline *iam*-PP sample, instead, show elastic behavior in a much larger deformation range, nearly coincident with the maximum deformation achieved during the first stretching of unoriented films. In fact, since the unoriented films can be stretched up to very high deformation (up to 1200%) and experience a nearly total recovery of the initial dimension upon

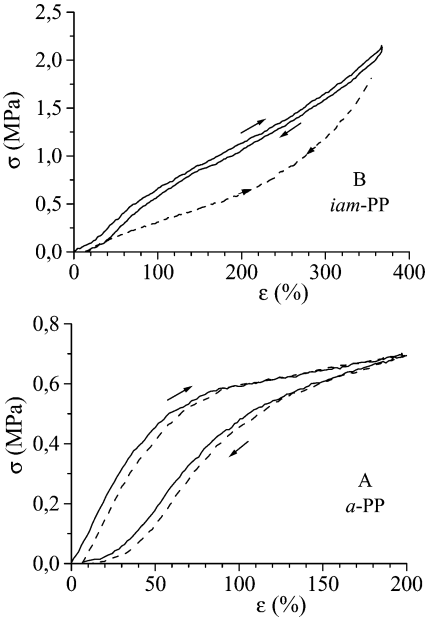

Figure 8. Stress−strain hysteresis cycles recorded at room temperature, composed of stretching and relaxation (at controlled rate) steps according to the direction of the arrows, for stress-relaxed fibers of the samples *a*-PP (A) and *iam*-PP (B). The stress-relaxed fibers have been prepared by stretching compression molded films, of initial length L_0, up to 300% elongation (final length $L_f = 4L_0$) for the sample *a*-PP and 600% deformation (final length $L_f = 7L_0$) for the sample *iam*-PP and then removing the tension. In the hysteresis cycles, the stretching steps are performed stretching the fibers up to final lengths $L_f = 4L_0$ and $7L_0$ for the samples *a*-PP and *iam*-PP, respectively. The first hysteresis cycle (continuous lines) and curves averaged for at least four cycles successive to the first one (dashed lines) are reported.

removing the tension (the tension set observed after the first stretching being very low even for large deformation, see Table 3), the oriented fibers give elastic response in a large range of deformation, up to the maximum deformation achieved during the preparation of the fibers.

As discussed above, in fibers of the *iam*-PP sample the elastic recovery observed upon releasing the tension is associated with a polymorphic transformation occurring inside the crystalline domains. Crystalline modifications of i-PP very close to the α form, having a high fraction of α-like facing with parallel chains, formed during stretching, transform back into more disordered modifications upon releasing the tension (Figure 6). These small crystalline domains act as physical knots in an amorphous matrix. The chains belonging to the amorphous phase, connecting the crystalline regions, undergo a reversible conformational transition between the entropically favored disordered random coil conformation in the unstretched state and the extended conformation in the stretched state. Therefore, the entropic effect due to this conformational transition is responsible for the elasticity. These amorphous chains

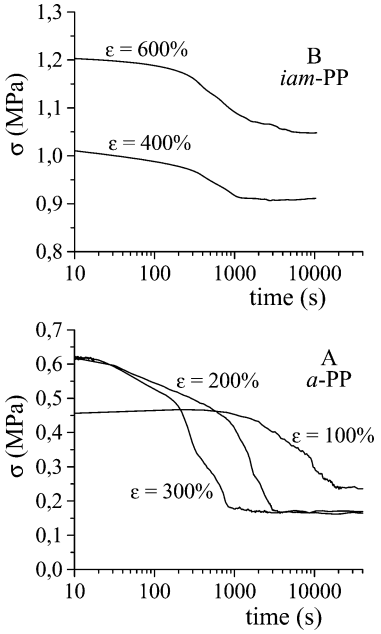

Figure 9. Stress−relaxation curves of *a*-PP (A) and *iam*-PP (B) samples. The values of the stress are reported as a function of time for compression molded films after application of instantaneous strains of 100%, 200%, and 300% for the *a*-PP sample (A) and 400% and 600% for the *iam*-PP sample (B).

are entangled and connect, as tie-chains, the small crystalline domains. They act as springs between the crystals being well-oriented and in extended conformation in the stretched state and return in the disordered coil conformation when the tension is removed.

Stress-relaxation experiments have been performed at room temperature on the compression molded films of *a*-PP and *iam*-PP samples to test the strength of these materials in conditions of application of a deformation for long time. The values of the stress are recorded as a function of the time after application on compression molded films of instantaneous strains of 100, 200, and 300% for the *a*-PP sample, and 400% and 600% for the *iam*-PP sample (Figure 9).

The samples show a typical behavior of viscoelastic materials with a decrease of the value of the stress with time at constant deformation (Figure 9). For the amorphous *a*-PP sample, a high loss of the stress of about 50% for small deformations ($\epsilon = 100\%$) and nearly 70% for higher deformations ($\epsilon = 200$ and 300%) is observed (Figure 9A). The decrease of the stress occurs after 1000 s for small instantaneous deformation ($\epsilon = 100\%$) and after 100−200 s for higher deformations ($\epsilon = 200$ and 300%). Then, the stress remains constant at values of about 0.2 MPa.

For the semicrystalline iam-PP sample, a smaller loss of the stress of nearly 10% after 1000 s, regardless of the instantaneous deformation, is observed (Figure 9B). Then, the stress remains constant at values of nearly 1 MPa for a long time. These data confirm the previous observations that, although the semicrystalline *iam*-PP sample has a molecular weight not as high as that of the amorphous *a*-PP sample, it shows elastic properties with remarkable values of strength even when stresses are applied for long time. The amorphous *a*-PP sample shows instead lower strength and high loss of the strength in short time because of disentanglement of the chains upon application of stresses for long time.

Concluding Remarks

The C_{2v}-symmetric and the chiral C_2-symmetric *ansa*-zirconocene catalysts (**5** and **6** in Chart 2) produce high molecular weight atactic polypropylene (*a*-PP) and poorly isotactic polypropylene (*iam*-PP) of medium molecular weight, respectively. Both samples show elastic properties, whereas only *iam*-PP is able to crystallize.[22,24]

The as-prepared poorly isotactic *iam*-PP sample is actually amorphous and does not crystallize by cooling the melt to room temperature. It slowly crystallizes by aging at room temperature or by stretching. A maximum degree of crystallinity of nearly 16% is achieved. The structural analysis has shown that the *iam*-PP sample crystallizes in the bulk and in stretched fibers in a continuum of disordered modifications intermediate between α and γ forms (Figure 1). The disorder corresponds to defects in the stacking of bilayers of chains along the b_α axis. Consecutive bilayers may face each other with the chain axes either parallel (like in the α form) or nearly perpendicular (like in the γ form). The amount of α-like (with parallel chains) and γ-like arrangements (with perpendicular chains) present in these structures changes with the degree of deformation. Structures similar to the γ form, present in unoriented films, transform by stretching at high deformation into structures more similar to the α form.

This crystallization mode of i-PP explains the capability of the *iam*-PP sample to crystallize, even though the stereoregularity of the sample is very low. Most of the defects of strereoregularity (*rr* triads) can be easily tolerated at low cost of conformational and packing energy in the crystal lattices of α and γ forms and of the α/γ disordered modifications. The inclusion of *rr* defects induces the crystallization in disordered modifications intermediate between α and γ forms of i-PP and gives a possible explanation of the development of crystallinity in i-PP samples having very low stereoregularity and, as a consequence, of the elastic properties.

The analysis of the mechanical properties has shown that the amorphous *a*-PP sample presents elastic behavior only in small deformation range (up to 300% strain). The elasticity arises from the physical network generated by the high degree of entanglement of the polymeric chains because of the high molecular weight of the sample. The presence of these physical knots, associated with the high viscosity due to the high molecular weight, prevents the viscous flow of the chains when the sample is stretched up to 300% deformation, and a good elastic recovery is observed upon releasing the tension. When the sample is stretched at deformations higher than 300% disentanglement of the chains occurs, producing viscous flow and the sample loses the elastic properties.

The semicrystalline *iam*-PP sample presents instead good elastic properties in a large range of deformation. Although this sample has a molecular weight lower than that of the amorphous *a*-PP sample, it shows better elastic properties. However, the *iam*-PP sample in the amorphous state, before crystallization, presents much poorer elastic properties than the *a*-PP sample because of the lower molecular weight. After crystallization, it shows better elastic properties with higher strength, notwithstanding the lower molecular weight because of the presence of crystallinity.

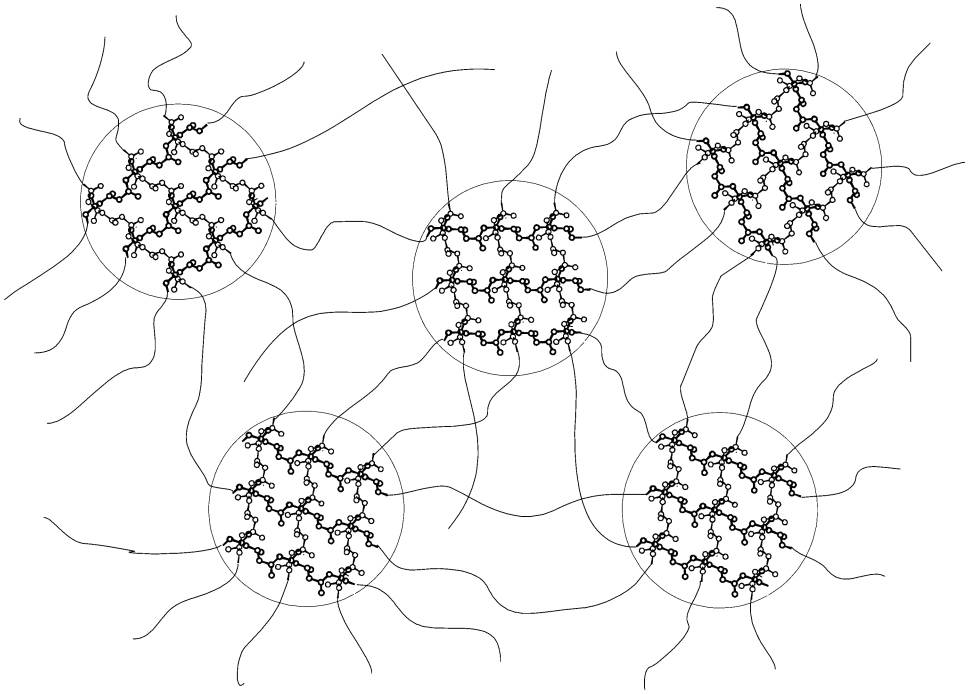

Figure 10. Model of the elastomeric lattice in the semicrystalline *iam*-PP sample. The crystalline domains act as knots of the elastomeric network. They are characterized by α/γ disordered modifications containing i-PP chains oriented along two nearly perpendicular directions. The amorphous polymeric tie-chains connecting the different crystalline domains come out from crystals along two perpendicular directions.

The elasticity of the poorly crystalline *iam*-PP sample is therefore due to the presence of small crystalline domains in the amorphous matrix, which act as physical knots of the elastomeric lattice, preventing the viscous flow of the chains and giving a typical thermoplastic elastomeric behavior with remarkable value of the strength. The chains belonging to the amorphous phase, connecting the crystalline regions, undergo a reversible conformational transition between the entropically favored disordered random coil conformation in the unstretched state and the extended conformation in the stretched state. Therefore, the entropic effect due to this conformational transition is responsible for the elasticity. These amorphous chains are entangled and connect, as *tie-chains*, the small crystalline domains. They act as springs between the crystals being well-oriented and in extended conformation in the stretched state and return in the disordered coil conformation when the tension is removed. A model of the elastomeric lattice in the semicrystalline *iam*-PP sample is shown in Figure 10.

As discussed above, the elastic recovery observed in fibers of the *iam*-PP sample upon releasing the tension is associated with a polymorphic transformation occurring inside the crystalline domains. Crystalline modifications of i-PP very close to the α form, having a high fraction of α-like arrangements with parallel chains formed during stretching, transform back upon releasing the tension into more disordered modifications. These small crystalline domains are therefore always characterized by α/γ disordered modifications, with a certain fraction of parallel or perpendicular chains depending on the degree of deformation (Figure 10). Crystals in the pure α form, with all parallel chains, are never obtained even at very high deformation.[24] The presence of defects characterized by a certain amount of bilayers with perpendicular chains is therefore unavoidable. For these reasons, the small crystalline domains containing these defects represent very special knots of the elastomeric lattice because, as shown in Figure 10, the amorphous tie-chains connecting the different crystalline regions come out from crystals along two perpendicular directions, giving a speculative idea of a more efficient connectivity and a more stable network.

Acknowledgment. Financial supports from Basell Ferrara, Italy and from the "Ministero dell'Istruzione, dell'Università e della Ricerca" (PRIN 2002 and Cluster C26 projects) are gratefully acknowledged. We thank Dr. Luigi Resconi of Basell for providing the polymer samples and for having stimulated this study.

References and Notes

(1) Ewen, J. A.; Elder, M. J.; Jones, R. L.; Haspeslagh, L.; Atwood, J. L.; Bott, S. J.; Robinson, K. *Makromol. Chem., Macromol. Symp.* **1991**, *48/49*, 253.
(2) Brintzinger, H. H.; Fischer, D.; Mülhaupt, R.; Rieger, B.; Waymouth, R. M. *Angew. Chem., Int. Ed. Engl.* **1995**, *34*, 1143.
(3) Kaminsky W. *Macromol. Chem. Phys.* **1996**, *197*, 3907.
(4) Resconi, L.; Cavallo, L.; Fait, A.; Piemontesi, F. *Chem. Rev.* **2000**, *100*, 1253.
(5) Natta, G.; Mazzanti, G.; Crespi, G.; Moraglio, G. *Chim. Ind. (Milan)* **1957**, *39*, 275.
(6) Natta, G. U.S. Patent 3,175,999, 1965.
(7) Natta, G. *J. Polym. Sci.* **1959**, *34*, 531. Natta, G.; Mazzanti, G.; Crespi, G.; Moraglio, G. *Chim. Ind. (Milano)* **1957**, *39*, 275.
(8) Collette, J. W.; Tullock, C. W. (Dupont) U.S. Patent 4335225, 1982. Tullock, C. W.; Mülhaupt, R.; Ittel, S. D. *Makromol. Chem., Rapid Commun.* **1989**, *10*, 19. Tullock, C. W.; Tebbe, F. N.; Mülhaupt, R.; Ovenall, D. W.; Setterquist, R. A.; Ittel, S. D. *J. Polym. Sci., Polym. Chem.* **1989**, *27*, 3063.
(9) Collette, J. W.; Tullock, C. W.; MacDonald, R. N.; Buck, W. H.; Su, A. C. L.; Harrel, J. R.; Mülhaupt, R.; Anderson, B. C. *Macromolecules* **1989**, *22*, 3851.
(10) Collette, J. W.; Ovenall, D. W.; Buck, W. H.; Ferguson, R. C. *Macromolecules* **1989**, *22*, 3858.
(11) Coates, G. W.; Waymouth, R. M. *Science* **1995**, *267*, 217.

(12) Hu, Y.; Krejchi, M. T.; Shah, C. D.; Myers, C. L.; Waymouth, R. M. *Macromolecules* **1998**, *31*, 6908. Lin, S.; Waymouth, R. M. *Acc. Chem. Res.* **2002**, *35*, 765.
(13) Mallin, D. T.; Rausch, M. D.; Lin, Y.-G.; Dong, S.; Chien, J. C. W. *J. Am. Chem. Soc.* **1990**, *112*, 2030. Chien, J. C. W.; Llinsas, G. H.; Rausch, M. D.; Lin, G.-Y.; Winter, H. H. *J. Am. Chem. Soc.* **1991**, 113, 8569. Chien, J. C. W.; Llinsas, G. H.; Rausch, M. D.; Lin, G.-Y.; Winter, H. H., Atwood, J. L.; Bott, S. G. *J. Polym. Sci., Polym. Chem.* **1992**, *30*, 2601. Llinas, G. H.; Day, R. O.; Rausch, M. D.; Chien, J. C. W. *Organometallics* **1993**, *12*, 1283.
(14) Gauthier, W. J.; Collins, S. *Macromol. Symp.* **1995**, *98*, 223.
(15) Gauthier, W. J.; Corrigan, J. F.; Taylor, N. J.; Collins, S. *Macromolecules* **1995**, *28*, 3771.
(16) Gauthier, W. J.; Collins, S. *Macromolecules* **1995**, *28*, 3779.
(17) Bravakis, A. M.; Bailey, L. E.; Pigeon, M.; Collins, S. *Macromolecules* **1998**, *31*, 1000.
(18) Dietrich, U.; Hackmann, M.; Rieger, B.; Klinga, M.; Leskelä, M. *J. Am. Chem. Soc.* **1999**, *121*, 4348. Müller, G.; Rieger, B. *Prog. Polym. Sci.* **2002**, *27*, 815. Rieger, B.; Troll, C.; Preuschen, J. *Macromolecules* **2002**, *35*, 5742.
(19) Resconi, L.; Jones, R. L.; Rheingold, A.; Yap, G. P. A. *Organometallics* **1996**, *15*, 998.
(20) Resconi, L. Synthesis of atactic polypropylene using metallocene catalysts. In *Metallocene-Based Polyolefins. Preparation, Properties, Technology*; Kaminsky, W., Scheirs, J., Eds.; Wiley: 1999; p 467.
(21) Resconi, L.; Silvestri, R. In *The Polymeric Materials Encyclopedia*; Salamone, J. C., Ed.; CRC Press: Boca Raton, FL, 1996; p 6609.
(22) Balboni, D.; Moscardi, G.; Baruzzi, G.; Braga, V.; Camurati, I.; Piemontesi, F.; Resconi, L.; Nifant'ev, I. E.; Venditto, V.; Antonucci, S. *Macromol. Chem. Phys.* **2001**, *202*, 2010.
(23) Resconi, L.; Moscardi, G.; Silvestri, R.; Balboni, D. WO 00/01738 2000 Montell.
(24) Auriemma, F.; De Rosa, C.; Boscato, T.; Corradini, P. *Macromolecules* **2001**, *34*, 4815.
(25) De Rosa, C.; Auriemma, F.; Circelli, T.; Waymouth, R. M. *Macromolecules* **2002**, *35*, 3622.
(26) Auriemma, F.; De Rosa, C. *Macromolecules* **2002**, *35*, 9057.
(27) De Rosa, C.; Auriemma, F.; Circelli, T.; Longo, P.; Boccia, A. C. *Macromolecules* **2003**, *36*, 3465.
(28) Natta, G.; Corradini, P. *Nuovo Cimento Suppl.* **1960**, *15*, 40.
(29) Alamo, R. G.; Kim, M. H.; Galante, M. J.; Isasi, J. R.; Mandelkern, L. *Macromolecules* **1999**, *32*, 4050.
(30) Brückner, S.; Meille, S. V.; Petraccone, V.; Pirozzi, B. *Prog. Polym. Sci.* **1991**, *16*, 361.
(31) Brückner, S.; Meille, S. V. *Nature* **1989**, *340*, 455. Meille, S. V.; Brückner, S.; Porzio, W. *Macromolecules* **1990**, *23*, 4114.
(32) Geddes, A. J.; Parker, K. D.; Atkins, E. D. T.; Beighton, E. *J. Mol. Biol.* **1968**, *32*, 343.
(33) VanderHart, D. L.; Alamo, R. G.; Nyden, M. R.; Kim, M. H.; Mandelkern, L. *Macromolecules* **2000**, *33*, 6078.
(34) Starkweather, H. W., Jr.; VanCatledge, F. A.; MacDonald, R. N. *Macromolecules* **1982**, *15*, 1600.
(35) Nyden, M. R.; VanderHart, D. L.; Alamo, R. G. *Comput. Theor. Polym. Sci.* **2001**, *11*, 175.

MA0493372